MDPI

Article

Investigation into Red Emission and Its Applications: Solvatochromic N-Doped Red Emissive Carbon Dots with Solvent Polarity Sensing and Solid-State Fluorescent Nanocomposite Thin Films

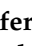Justin B. Domena [1], Ermin Celebic [1], Braulio C. L. B. Ferreira [1], Yiqun Zhou [1], Wei Zhang [1], Jiuyan Chen [1], M. Bartoli [2], A. Tagliaferro [2], Qiaxian Johnson [3], Bhanu P. S. Chauhan [3], Victor Paulino [1], Jean-Hubert Olivier [1] and Roger M. Leblanc [1,*]

[1]   Department of Chemistry, University of Miami, Coral Gables, FL 33146, USA
[2]   Department of Applied Science and Technology, Politecnico di Torino, 10129 Torino, Italy
[3]   Department of Chemistry, William Paterson University of New Jersey, 300 Pompton Rd, Wayne, NJ 07470, USA
*   Correspondence: rml@miami.edu

Abstract: In this work, a NIR emitting dye, *p*-toluenesulfonate (IR-813) was explored as a model precursor to develop red emissive carbon dots (813-CD) with solvatochromic behavior with a red-shift observed with increasing solvent polarity. The 813-CDs produced had emission peaks at 610 and 698 nm, respectively, in water with blue shifts of emission as solvent polarity decreased. Subsequently, 813-CD was synthesized with increasing nitrogen content with polyethyleneimine (PEI) to elucidate the change in band gap energy. With increased nitrogen content, the CDs produced emissions as far as 776 nm. Additionally, a CD nanocomposite polyvinylpyrrolidone (PVP) film was synthesized to assess the phenomenon of solid-state fluorescence. Furthermore, the CDs were found to have electrochemical properties to be used as an additive doping agent for PVP film coatings.

Keywords: carbon dots; red emission; solvatochromic; nanocomposite; thin film

1. Introduction

Carbon dots (CDs) have attracted increased attention in various biomedical areas such as in vitro/in vivo imaging, photodynamic and photothermal therapy [1–7]. When compared to typical organic dyes, CDs have the advantage of low cost, high biocompatibility and photostability, and amphiphilic behaviors [8–11]. Current efforts in developing red-emissive carbon dots as photosensitizers (PS) past 650 nm have been elusive [12]. The importance of this photophysical property is to surpass the requirement of the utilization of light within the red region to NIR-I window ranging between 650–950 nm, respectively for enhanced biological imaging [13,14]. A multitude of studies have sought to elucidate the synthetic methods to reach red emissive CDs, though few reach past the far-red region. Such efforts involve using carbon sources with features such as extended aromatic systems or heteroatoms (sulfur, nitrogen, and phosphorus) [15–22]. Specifically, the presence of heterocycles has been deduced to contribute to an increased degree of surface defects which effectively reduces the HOMO-LUMO energy gaps leading to a bathochromic shift of emission. In this study, we investigated the increased doping of nitrogen of 813-CDs by the introduction of different chain length PEI. To investigate the electronic transitions of the 813 CDs, the optical band gap energies of the respective CDs were elucidated by using the UV-vis spectrum converted to α vs energy plot by using Equation (1) instead of Tauc's plot.

$$\alpha = \frac{2.303\,A}{l} \qquad (1)$$

where α is denoted as the molar absorption coefficient at the resultant wavelength and is calculated from Beer-Lambert's relation according to Equation (1) such that A is the absorbance and l is the optical pathlength. The simple use of the Tauc approach is incorrect due to its applicability only to crystals, while CDs should be correctly modelled as large molecules [23–25]. Studies have suggested that intricate surface modifications are vital to develop red emissive CDs. Additionally, the interest in developing novel CDs from NIR dye sources has increased greatly [26]. This is due to the notion that when synthesizing a CD, the precursor is only partially broken down during the reaction, leaving moieties close to that of the original base structure. Hence, most of the conjugated network is retained resulting in a slight hypsochromic shift. As promising candidates, NIR fluorophores as precursors to red emissive CDs are of interest.

Until recently, post-synthetic parameters have been investigated to understand the influence of solvent polarity on the emissive properties of CDs [27–34]. Solvents of various polarities have discreet effects on the electronic transition of dipolar solutes. For example, when exposed to highly polar solvent, a fluorophore can exhibit two types of solvatochromism (positive or negative) [35,36]. Positive solvatochromism occurs due to a lower shift in the UV-vis transition energy resulting in a longer wavelength. This phenomenon is observed because the dipole moment of the molecule in ground state is smaller than that of the dipole moment in the excited state [37]. On the other hand, fluorophores exhibit negative solvatochromism due to a higher shift of UV-vis transition energy resulting in a shorter wavelength [38]. In this work, we propose that this feature of solvent polarity is important as CDs can be exploited in two ways: to produce a red shift in its optical properties, and to be used as a polarity sensing agent. Herein, we report the development of stable red emitting 813-CDs with polarity sensing capabilities.

Polyvinylpyrrolidone (PVP) has extensively been studied for its application in pharmaceuticals, electronics, cosmetics, and polymers [39–45]. Specifically, as a thin film composite, PVP, when polymerized with CDs, may have the feature to lock in place their emissive state [46–49], resulting in what is known as solid state fluorescence. There are few papers which address this phenomenon as carbon dots typically undergo fluorescence self-quenching in solid state due to aggregation [50,51]. Furthermore, these 813-CDs have been used with PVP to develop a red emitting thin film nanocomposite polymer which exhibits solid state fluorescence. We hypothesize that by introducing the CDs into a polymer matrix, the disabling of both the $\pi-\pi$ interaction and fluorescence resonance energy transfer (FRET) between neighboring CDs will be observed. These interactions are known to play a key role in fluorescence self-quenching of CDs in solid state. Another promising feature of CDs is their potential as a doping agent to enhance electrochemical behaviors in PVP films, namely coatings for battery cathodes.

Herein, we propose the synthesis of far-red emitting carbon dots from the NIR emitting dye, IR-813. In comparison to current NIR photosensitizers, CDs boast features such as thermal and photostability. The feature of these carbon dots stems from the passivation of PEI during synthesis which aids in two aspects: (1) to have increased water solubility, as carbon dots derived from dyes usually lack this characteristic; and (2) PEI as a polymer encases the dye during microwave irradiation to slow the thermal degradation of the dye [52]. A feature of CDs to be used biologically is dependent on their surface functionalization. Specifically, the surface of the CD can modulate the pathway of cellular uptake, intracellular trafficking, and cytotoxicity [53]. As a surface passivant, PEI is a highly favored cationic macromolecule for use in gene transfer therapy due to high transfection efficiency [54]. Additionally, PEI molecules interact with negatively charged proteins in cytoskeletons, such as actin and beta-tubulin [55]. Another important feature of selecting PEI for surface functionalization of CDs is to provide both a positive charge and to improve permeabilization of the plasma membrane. The literature further conjectures that PEI as a drug delivery vesicle or passivant can disrupt endosomal membranes through the well-known "proton sponge effect", which states that the presence of a weekly basic molecule may cause the endosome to burst. This facilitates the possible pathways that allow binding of the material

to DNA [56,57]. To further clarify our rationale for PEI as a choice for nitrogen content, the literature shows that the increase of PEI weight during synthesis serves as a facile method to increase the degree of amidation of a nanoparticle [58].

2. Experimental Section

2.1. Materials

Two polyethyleneimine (PEI), branched (MW: 600 and 25 K) and *p*-toluenesulfonate were procured from Sigma-Aldrich (St. Louis, MO, USA). Polyvinylpyrrolidone (PVP) was obtained from VWR (West Chester, PA, USA). All solvents used were HPLC grade including ethanol, acetic acid, dimethyl sulfoxide (DMSO), dimethylformamide (DMF), methylene chloride, chloroform, ethyl acetate, toluene, ether, and hexane which were purchased from Sigma-Aldrich (St. Louis, MO, USA), and were used as received without further purification. Deionized (DI) water used was ultrapure (type I) water which was purified using a Millipore Direct-Q 3 water purification system acquired from EMD Millipore Corporation. The purified water displayed a surface tension of 72.6 mN m^{-1}, a resistivity of 18.2 MW cm and a pH value of 7.0 ± 0.3 at 20.0 ± 0.5 °C. All the chemicals were used as received.

2.2. Synthesis of 813-CD-600 PEI

The 813-CDs were obtained by means of microwave pyrolysis of IR813 (0.100 g) and PEI MW 600 (0.050 g) as illustrated in Figure S1 (in the Supplementary Materials). To preface, the precursors were dispersed in a beaker containing 15 mL of methanol and sonicated for 1 min to ensure a homogenous mixture which was observed to exhibit a dark-green color. The solution of starting material was then placed in the microwave and set for 360 s at a power setting of 700 W. Post pyrolysis, it was observed that no solution remained, leaving a bright orange gel-like product, 813-CD (Figure S2A). The product was then purified by flash chromatography with an eluent system of 75% hexane, 5% methanol, and 20% ethyl acetate by volume (v:v:v), producing an orange-red product labelled 813-CD-600 PEI. To ensure a product with little to no solvent, a Buchi Rotavapor (Waterbath B-480) was used to eliminate all organic solvent impurities. The purified solution of 813-CDs was dried and re-dispersed in ultrapure (type I) deionized (DI) water. The dispersion was then frozen at −40 °C for 24 h and sequentially set for lyophilization for 72 h. Producing again, an orange-red gel-like product. These freeze-dried CDs were then used for study.

2.3. Synthesis of 813-CD-25K PEI

The 813-CDs were obtained by means of microwave pyrolysis of IR813 (0.100 g) and PEI MW 25K (0.050 g). The methodology for the synthesis of 813-CD-25K is the same as in Section 2.2. Post pyrolysis, it was observed that no solution remained, leaving a dark black-orange 813-CD (Figure S2B). The product was then purified by flash chromatography with the same eluent system as 813-CD-600 PEI, producing a dark green-orange product labeled 813-CD-25K PEI. These freeze-dried 813-CD-25K PEI CDs were also used in our study.

2.4. Synthesis of 813-CD-600 PEI/PVP Nanocomposite Thin Film

To synthesis 813-CD-600 PEI/PVP nanocomposite thin films, 500 mg of PVP were dissolved in 5 mL of ethanol and sonicated for 1 min. Next, 5.00 mg of 813-CD were also dispersed in 5 mL of ethanol and sonicated for 1 min. The now dispersed solution of 813-CDs was aliquoted into the prepared PVP ethanol solution at 1 mL intervals and was uniformly dispersed under stirring. The obtained mixture was poured into a glass Petri plate and dried for 24 h under ambient conditions in the dark to obtain the 813-CD/PVP film.

2.5. Characterization

UV-vis spectra were obtained from an Agilent Cary 100 UV-vis spectrophotometer. Photoluminescence (PL) characterization was performed on a Fluorolog HORIBA Jobin Yvon fluorometer with a slit width of 5 nm for excitation and emission. All optical charac-

terization spectra were obtained with quartz cells possessing an optical pathlength of 1 cm. Fourier-transform infrared (FTIR) spectroscopy data were obtained with a PerkinElmer FTIR (Frontier) spectrometer (Waltham, MA, USA) by using the attenuated total reflection (ATR) technique with air as background. The AFM images of 813-CDs were obtained with an Agilent 5420 atomic force microscope (Santa Clara, CA, USA) by using tapping mode. To perform AFM measurements, a drop of diluted 813-CDs aqueous solution was applied on a clean silica mica slide and air dried, which was then transferred to perform the screening using tapping mode. The tip used was silicon (length: 225 μm; thickness: 5 μm) manufactured from Nanosensors with a force constant of 15 N/m. The TEM was performed by using a JEOL 1200 EX TEM (Peabody, MA, USA). For TEM measurements, a drop of the 813-CDs solution was placed on a carbon coated copper grid and air-dried prior to examination. Scanning electron microscopy (SEM) images were taken at 15 KV accelerating voltage on a Hitachi SU1510. The Zeta potential was recorded on a Malvern Zetasizer nano-series. Electrochemical measurements were conducted using a PARSTAT 3000A potentiostat (Ametek Scientific Instruments, Berwyn, PA, USA) as reported in the literature [59].

3. Results and Discussion

3.1. UV-Vis Analysis of 813-CD 600 PEI

The detailed preparation of 813-CDs was described in Section 2. The UV-vis spectroscopy is a suitable tool to assess the electronic structure of conjugated systems. As expected, the absorption spectra of 813-CDs exhibited the typical absorption bands attributed to the $\pi-\pi*$ transitions of the C=C bond and the $n-\pi*$ transition of the C=O bond at 210 and 290 nm, respectively (Figure 1) [60,61]. A band at 375 was found to be similar to that of IR-813, which derives from the $n-\pi*$ transition of C=N functionalities present in the cyclic systems. Additionally, further bands were found at 450, 545, 590, 665, and 745 nm, respectively. These ranges are hypothesized to be due to the degradation of the cyclic structure of IR-813 to form new nitrogen-containing heterocyclic structures coordinated with PEI to form new emissive states [62–65]. However, the loss of conjugation is what leads to bands with a hypsochromic shift.
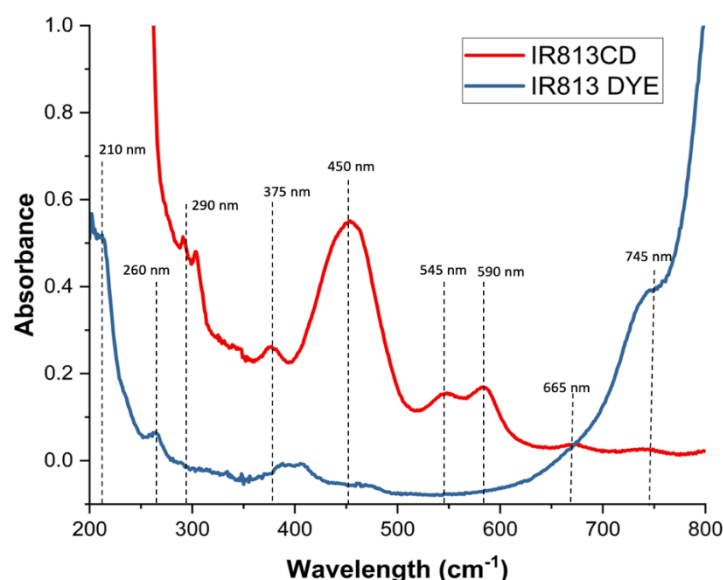

Figure 1. UV-vis analysis of 813-CDs and IR-813 dye.

3.2. Solvatochromic PL Behavior of 813-CD

Fluorescence spectroscopy is both an ideal and sensitive technique to supplement data from UV-vis to understand the fluorescent behavior of materials that absorb light. The farthest PL peak and its respective PL intensity in counts per second (CPS) of 813-CD-600

PEI (0.1 mg/mL) was recorded to assess the viability of the material in solvent polarity sensing techniques across a wide range of excitation in decreasing solvent polarities in Table 1 (water, ethanol, acetic acid, DMSO, DMF, methylene chloride, chloroform, ethyl acetate, toluene, ether, and hexane, respectively). The expected result was to produce CDs that retained optical properties similar to IR-813, which has notable emission peaks at 600 and 827 nm, respectively. We hypothesized that there may be degradation of the dye during the synthetic process, resulting in slight loss of conjugation. It is this decrease in conjugation that contributes to an increase of the energy band gap, producing a hypsochromic shift. Interestingly, this behavior was observed when the PL of the 813-CDs were excited between 380 to 600 nm, at 20 nm intervals in comparison to IR-813 (Figures S3 and S4). To our surprise, the most polar solvent (water) 813-CDs were found to possess far-red emission at 698 with a PL intensity of 1.5×10^6 (CPS). Interestingly, 813-CDs were found to have a clear isosbestic point at 575 nm. This finding is important because it means that there will be no change in the optical property at a set wavelength and hence, a uniformity in optical properties across the size distribution of CDs. This agrees with our prior hypothesis regarding the emissive origin of our CDs. As the 813-CDs were introduced to environments of decreasing solvent polarity, we started to observe negative solvatochromism. In ethanol, a hypsochromic shift was immediately observed as the farthest emissive peak was found at 650 nm with a PL intensity of 1.4×10^6 (CPS). The same trend occured as the 813-CDs were exposed to environments with even lower solvent polarity. In acetic acid, the PL shifted to 655 nm with a slight increase of PL intensity (1.9×10^6 (CPS)). The DMSO possessed PL at 610 nm and had a quite drastic decrease of PL intensity of 5.0×10^5 (CPS). Serving as the midway point of decreasing polarity, both DMF and methylene chloride produced the familiar PL peak at 655, but had a noticeable decrease of PL intensity to 1.1×10^6 and 1.0×10^6 (CPS), respectively. In chloroform, the 813-CDs emitted at 653 nm, but drastically dropped in PL intensity to 2.5×10^5 (CPS). Following the same trend, ethyl acetate, ether, and toluene had observed PL shifts to 650 nm followed by low PL intensities of 8.0×10^5, 7.2×10^5, and 3.8×10^5 (CPS), respectively. Notably, in hexane (the lowest polarity), the farthest emissive peak was found to be at 590 nm, meanwhile having the low PL intensity of 4.5×10^5 (CPS).

Table 1. Optical data of 813-CDs (farthest PL and intensity) and solvents used with their respective polarity index.

OPTICAL ANALYSIS OF 813 CDS IN VARIOUS SOLVENTS OF DECREASING POLARITY			
SOLVENT	**Polarity Index (P)**	**Farthest PL (nm)**	**PL Intensity (CPS)**
WATER	1.00	698	$1.5 * 10^6$
ETHANOL	0.654	650	$1.4 * 10^6$
ACETIC ACID	0.648	655	$1.9 * 10^6$
DMSO	0.444	610	$5.0 * 10^5$
DMF	0.386	655	$1.1 * 10^6$
METHYLENE CHLORIDE	0.309	655	$1.0 * 10^6$
CHLOROFORM	0.259	653	$2.5 * 10^5$
ETHYL ACETATE	0.228	650	$8.0 * 10^5$
ETHER	0.117	650	$7.2 * 10^5$
TOLUENE	0.099	650	$3.8 * 10^5$
HEXANE	0.009	590	$4.5 * 10^5$

To address the decrease in PL intensity with decreasing solvent polarity, we hypothesized that in more polar solvents there is the presence of aggregation induced emission (AIE) by particles. This phenomenon leads to more intense emissions at aggregated states in comparison to conventional aggregation fluorescence quenching mechanisms displayed by CDs [66]. From the results of the fluorescence study in various solvents, we propose a schematic illustration of the emission mechanism from 813-CDs in solvents of decreasing polarity (Figure 2). We hypothesized that behavior of the excited-state of 813-CDs is

dictated by the solute-solvent interactions of various polarities. Specifically, under excitation the solvent molecules have the opportunity to rotationally reorient to stabilize the excited-state dipole moment. This phenomenon as depicted is known as solvent relaxation, which is a key feature of both positive and negative solvatochromism [67–69]. Under this condition, we believe that 813-CDs experience a lowering of the energy of their excited state. Post-emission, the excited 813-CD returns to ground state. According to the literature, as the emission of CDs are linked to their $\pi \rightarrow \pi^*$ transition, the polarity of the solvent used will result in a reduction of energy of the first excited state (S_1) than that of the ground state (S_0). Effectively, as solvent polarity increases, the energy gaps between S_0 and S_1 are reduced resulting in longer emitted wavelengths. This phenomenon is attributed to the behavior of more polar solvents to enhance the electron cloud density of the CD's sp^2 domain which modulates the $\pi \rightarrow \pi^*$ electron transition [70]. We also observed the presence of the double-peaked nature of the 813-CDs. We hypothesized that this characteristic is due to a mix of the carbon core state (600 nm) and surface defects from PEI on the surface (697 nm). This is attributed to the transition of a higher singlet electronic state (S_2) undergoing internal conversion to a lower singlet electron state S_1 before returning to S_0. As we observed the drastic red-shifts of 813-CD-25K PEI, the idea of emissive states due to surface defects made sense as the double-band peak was not consistent in comparison to 813-CD-600 PEI having red shifts as far as 776 nm [71].
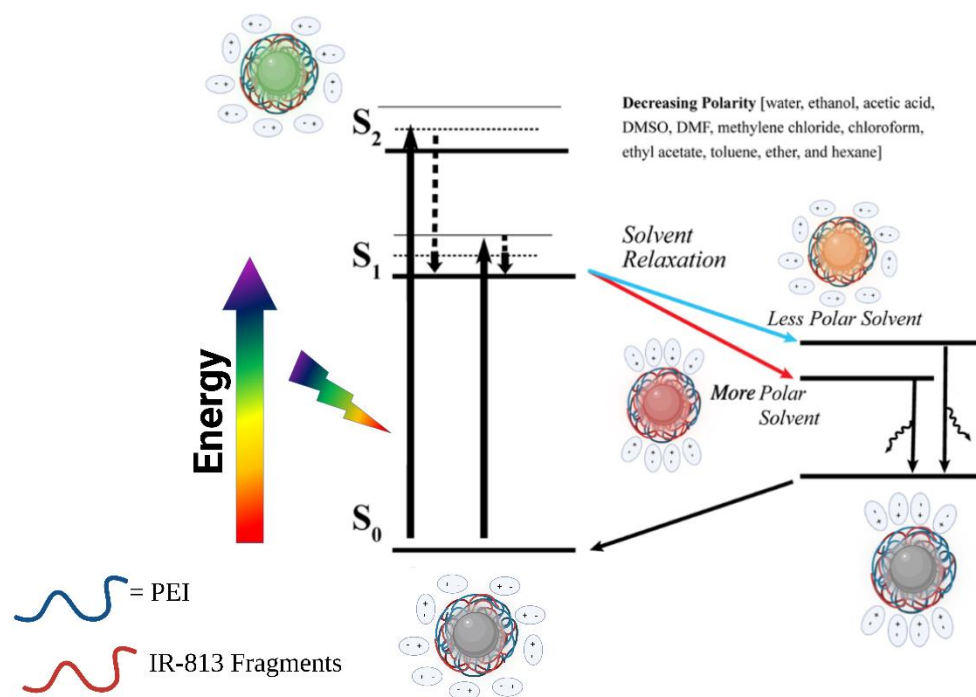

Figure 2. Schematic illustration of the emission mechanism from 813-CDs in solvents of decreasing polarity. Created with BioRender.com, accessed on 1 January 2023.

3.3. Optical Manipulation of 813CDs: 600 PEI vs. 25K PEI

To understand the influence of nitrogen content on the optical properties of the 813-CDs, α vs energy plot was developed as previously described, to reveal favorable insight into the electronic transitions between that of 813-CD 25K PEI and 813-CD 600 PEI via UV-vis spectra. The UV-vis data used in the α vs energy plot for determining the HOMO-LUMO energy gap (Δ_{HL}) are provided in Figure S5A,B. An analysis of 813-CD 25K PEI revealed that there were four main electronic transitions between the HOMO-LUMO states of the CD at Eg values of 5.02, 4.29, 2.35, and 2.26 eV, respectively (Figure 3A,B). We propose that these electronic transitions are due to the type of doped group, such as intrinsic carbon, graphitic nitrogen, carbonyl, and increased surface amines present, respec-

tively. Our premise is that the increased amount of surface defects from the orientation of nitrogen-based cyclic structures and amines on the surface of the CDs results in the lowering of the energy band gap; thus, causing the emission to be red shifted as the stokes shift range changes. To validate our hypothesis, 813-CD 600 PEI was then screened as the material of choice for α vs energy plot for determination as there was less nitrogen present in the same reaction conditions. Therefore, we expected that the band gaps overall would increase slightly. As expected, the analysis of 813-CD 600 PEI revealed that there were four electronic transitions between the HOMO-LUMO states of the CD that resembled that of the prior α vs energy plot. Only the Δ_{HL} was slightly larger, providing Eg values of 5.26, 4.34, 4.01, and 2.75 eV, respectively (Figure 3C,D). This observation made sense as even though there were the same type of doped groups present (intrinsic carbon, graphitic nitrogen, carbonyl, and surface amines present, respectively), with the lowering of nitrogen content, there were fewer surface defects state present which would lead to a higher energy band gap.
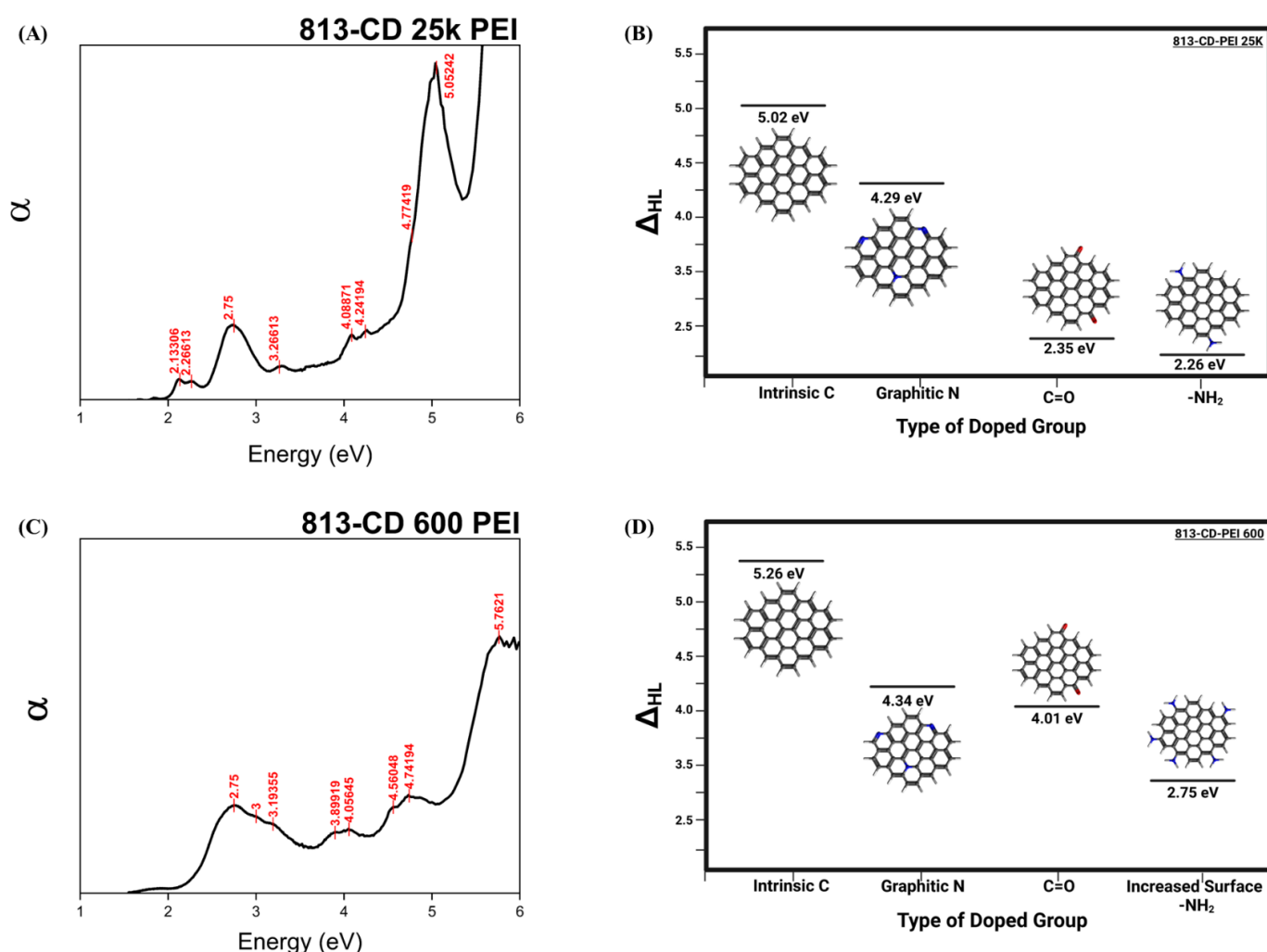

Figure 3. α vs energy plot of (**A**) 813-CD 25k PEI. (**B**) model representation of Δ_{HL} versus type of doped group of 813-CD 25k PEI. (**C**) α vs energy plot of 813-CD 600 PEI. (**D**) Model representation of model representation of Δ_{HL} versus type of doped group of 813-CD 600 PEI. Created with BioRender.com, accessed on 1 January 2023.

Subsequently, the PL properties between both 813-CD 25K PEI and 813-CD 600 PEI in water were studied to reveal how the Δ_{HL} correlates to the fluorescence capabilities. An observation of the PL spectrum of 813-CD 25K PEI postulates that the lowered band gap as determined by the α vs energy plot leads to the far-red emission at 723 nm (Figure 4A).

A second emissive peak was also observed at 600 nm, which decreased in intensity as the excitation wavelength was swept from 400 to 780 nm in 20 nm intervals, respectively. Interestingly, 813-CD 25K PEI was found to exhibit excitation dependence which is common with CDs that contain increased surface defects. Additionally, the normalized PL spectrum revealed that as the excitation wavelength is increased, the far-red emissive peak is further red shifted as far as 776 nm (Figure 4B). As expected, the PL spectrum of 813-CD 600 PEI was quite different regarding its far-red peak which was observed at 697 nm (Figure 4C). This result was expected in correlation to the α vs energy plot which suggests that the Δ_{HL} is at a higher value. At lower excitation wavelengths, 813-CD 600 PEI exhibited excitation dependence with rising emissive peaks at 600, 557, 510, and 445 nm, respectively (Figure 4D). We posited that during synthesis, the smaller chained PEI formed a variety of heterocyclic structures at the surface of the CD which led to the PL behavior as described.
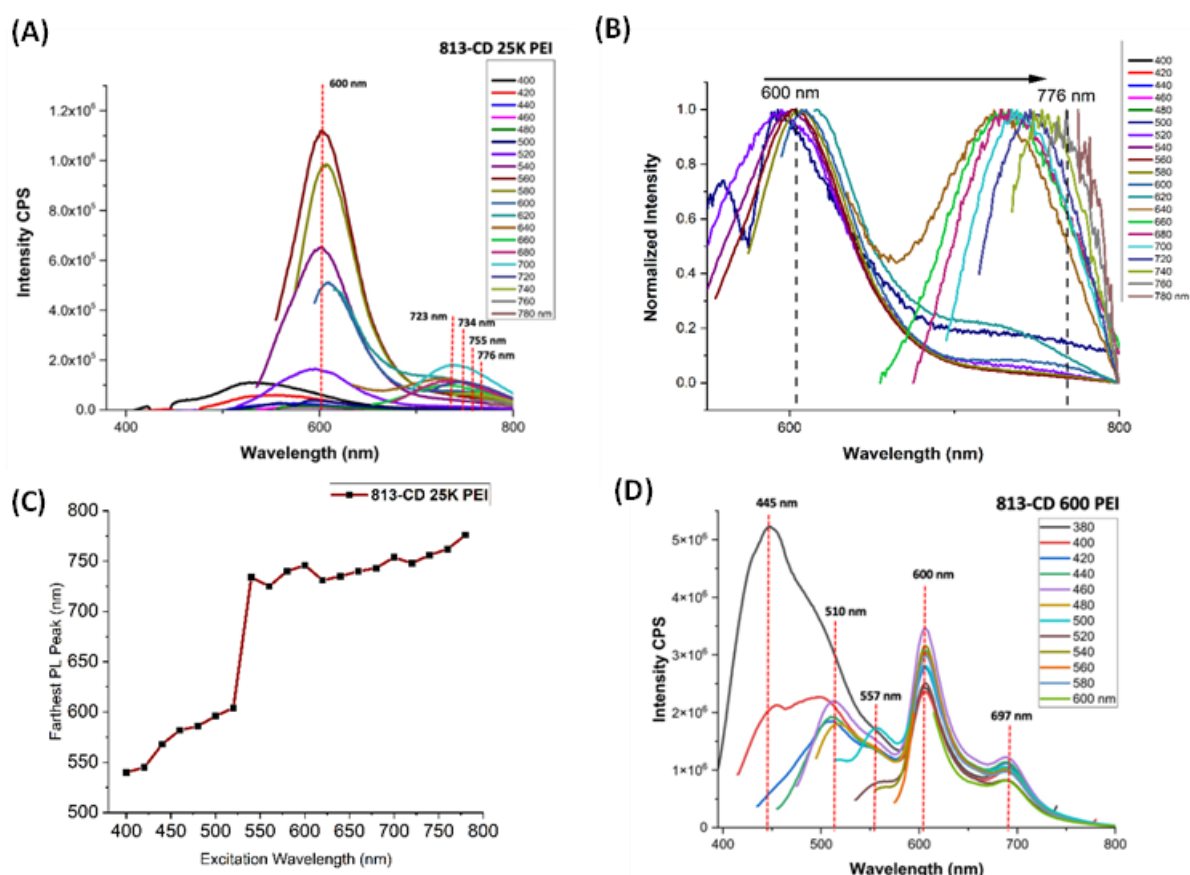

Figure 4. PL spectra of 813-CDs. (**A**) PL spectrum of 813-CD 25k PEI. (**B**) Normalized PL spectrum of 813-CD 25k PEI. (**C**) Plot of the second PL peak for 813-CD-25K PEI vs. excitation wavelength (nm). (**D**) PL spectrum of 813-CD 600 PEI.

There are quite a few perspectives on what factors serve as the emissive origin of CDs. All reasons point towards factors that are outside the realm of quantum confinement that associate the emissive shifts of well-defined nanoparticles according to size. The structure-property relationship of carbon dots is vague, leading to challenges in elucidating the source of emission. In fact, there are three models currently debated as plausible mechanisms for emission in CDs, i.e., carbon core states, surface states, and molecular fluorescence. Neither are well defined due to the diversity (size distribution) of CDs which cannot be isolated into just one uniform product. The CDs are a heterogenous distribution of different-sized particles that have the same emissive peak, loosely displaying the quantum size effect. Our line of thought stems from a mix of both carbon core and surface states of carbon dots. We posited that 813-CD-600 PEI may have more sp^2 domain sizes (carbon core state behavior)

which correlates to the slight size increase, though does not particularly contribute towards red emission [72]. This idea is corroborated by 813-CD-25k PEI which boasts farther red emission, yet has a smaller, more uniform size distribution. Hence, we hypothesized that the CD's emission may be linked to surface defects states of the CDs due to the protection of PEI of IR-813 [73].

The FTIR serves as a powerful tool to qualitatively analyze both the core and the functional groups that passivate the surface of CDs, which typically contain oxygen and nitrogen functional groups. A comparative analysis of 813-CDs and the starting material was performed to reveal insight into the surface of the CD (Figure 5). At first glance, both 813-CD 600 and 25K PEI have similar peaks. Upon analysis of 813-CDs, the intense peaks at 1335–1372 cm^{-1} and 1030–1070 cm^{-1} are due to the asymmetric S=O and sulfoxide stretching vibrations, respectively. This characteristic makes sense as there would be sulfoxide moieties present from the IR-813 precursor, which have the same respective peaks. These results suggest that 813-CDs retain most functionality from IR-813. A range between 3000–3100 cm^{-1} is attributed to the C-H stretching of the sp^2 carbon species, which make up the carbonized network of 813-CDs. Additionally, the broad peak at 3480 cm^{-1} is attributed to stretching vibrations of O-H (trace water) present, as well as the medium peak at 2850–3000 cm^{-1} indicative of C-H stretching of the alkane groups due to PEI present during the synthetic process, confirming the availability of these groups on the surface of the 813-CDs. The peak at 3300 cm^{-1} is ascribed to N-H (secondary) group on the surface of the 813-CDs due to PEI. It is hypothesized that these groups, which are abundant on the surface, are responsible for the high solubility of 813-CDs in water. This finding was reinforced through the analysis of 813-CD 25K PEI that had a more apparent N-H peak at 3300 cm^{-1}, attributed to the increase of nitrogen from the larger chain size, as well as more trace water found at 3480 cm^{-1}.
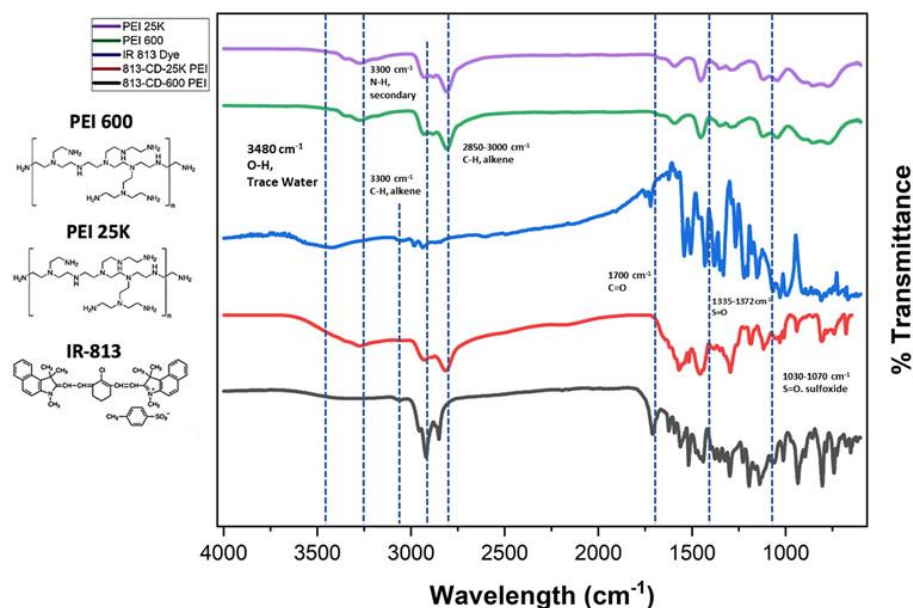

Figure 5. FTIR off-set spectra of PEI 25K, PEI 600, IR-813 dye, 813-CD-25k PEI, and 813-CD-600 PEI, respectively.

Functional moieties of two types of CDs can be identified and quantified by TGA and DTG analyses by their unique decomposition temperatures in reference to those of precursors. In general, the TGA of CDs and PEI (Figure 6A) showed similar thermal decomposition trends across different temperatures, which demonstrates a structural similarity among CDs and PEI. In comparison, the TGA of IR-813 exhibited more variations between 40–250 °C, which corresponds to a complicated structure. In addition, the differences of CDs and their precursors are displayed by the DTG (Figure 6B) and show that: (1) IR-813 has six decomposition stages: 40–127, 127–200, 200–248, 248–376, 376–463, and 463–673 °C;

(2) PEI 600 has two decomposition steps: 40–463, and 463–673 °C; (3) PEI 25K has two decomposition steps: 40–376, and 376–673 °C; (4) the CDs (CD-PEI 600) possess four decomposition periods: 40–127, 127–248, 248–463, and 463–673 °C; (5) the CDs (CD-PEI 25K) possess four decomposition periods: 40–200, 200–376, 376–463, and 463–673 °C; (6) both the DTG of PEG 600 and 25K generally show two decomposition stages, but different ranges indicate the effect of molecular weight on the thermostability of polymers; and (7) with the DTG of a well-established CD species as reference, any peaks between 40–127 °C indicate the loss of water molecules adsorbed on CDs. The mass loss at 127–200 °C suggests the loss of water molecules generated through intramolecular dehydration condensation reactions. The stage between 200–248 °C is attributed to the decomposition of edge-plane oxygen-containing functional groups. The stage at 248–376 °C is due to the decomposition of relatively stable oxygen-containing functional groups, and sublimation of small carbon frameworks. The stage at 376–463 °C indicates the decomposition of amines. Eventually, the stage at 463–673 °C indicates the decomposition of graphene-like structures; (8) therefore, during 40–127 °C, IR-813 and CDs (CD-PEI 600) showed desorption of moisture by 6 and 9%, respectively. In addition, in the corresponding TGA (Figure 6A), mass loss was observed among all the other samples, which was expected due to the presence of amines; (9) during 127–200 °C, CD-PEI 600 and CD-PEI 25k exhibited 13% and 12% mass loss of water molecules, respectively, formed through intramolecular dehydration condensation reactions. However, since intramolecular dehydration condensation reactions cannot occur in PEI, during this period, both PEI did not display significant mass loss. Furthermore, IR-813 contains perchlorate anions, so the mass loss is hypothesized to be evaporation of perchloric acid considering its boiling point at 203 °C; (10) the peak shown in the DTG of IR-813 between 200–248 °C indicates the loss of oxygen-containing functional moieties formed during the process of dye decomposition (Figure 6B); (11) sharp decompositions of relatively stable oxygen-containing functional groups and carbon frameworks were observed in all the samples during 248–376 °C, and the corresponding mass percentages in IR-813, PEI 600, PEI 25K, CD-PEI 600, and CD-PEI 25K are 40%, 59%, 85%, 30%, and 61%, respectively; (12) subsequently, mass losses occurred during 376–463 °C due to the decomposition of amines and the mass losses were 11%, 8%, 3%, 11%, and 5% for IR-813, PEI 600, PEI 25K, CD-PEI 600, and CD-PEI 25K, respectively; (13) and in the last stage between 463–673 °C and above 673 °C, mass losses of 30%, 18%, 7%, 27%, and 13% were obtained for IR-813, PEI 600, PEI 25K, CD-PEI 600, and CD-PEI 25K, respectively, due to the decomposition of aromatic structures.
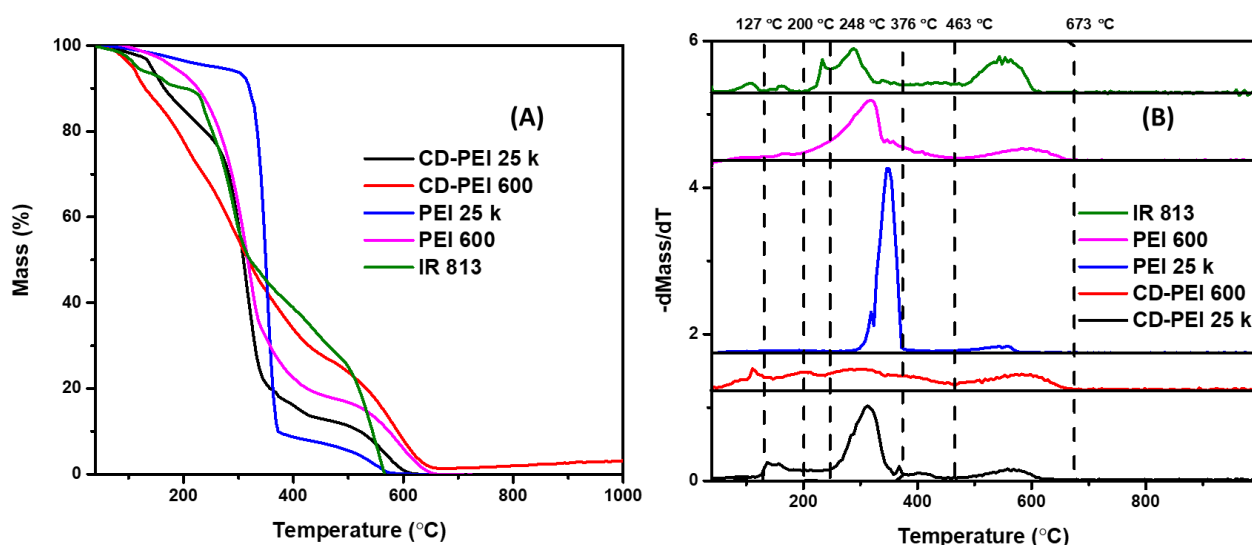

Figure 6. TGA (**A**) and DTG (**B**) of CDs and precursors including IR-813, PEI 600 and 25K.

Preliminary consideration of the structure should be based on both TGA and FT-IR data. As shown by TGA data, the aromatics domains represent a relevant amount of both 813-CDs produced by using both PEI 600 and 25 K, and they are due to native aromatic moieties of carbon dots and piperazine-like structure formed during the degradation of PEI [74]. Additionally, IR analysis shows the signal of sulphate proving the persistence of tosyl residues inside the 813-CDs.

Accordingly, we assumed the simultaneous occurrence of three pathways regarding the evolution of PEI, IR-813 and tosyl residues during the production of 813-CDs, as reported in Figure 7.
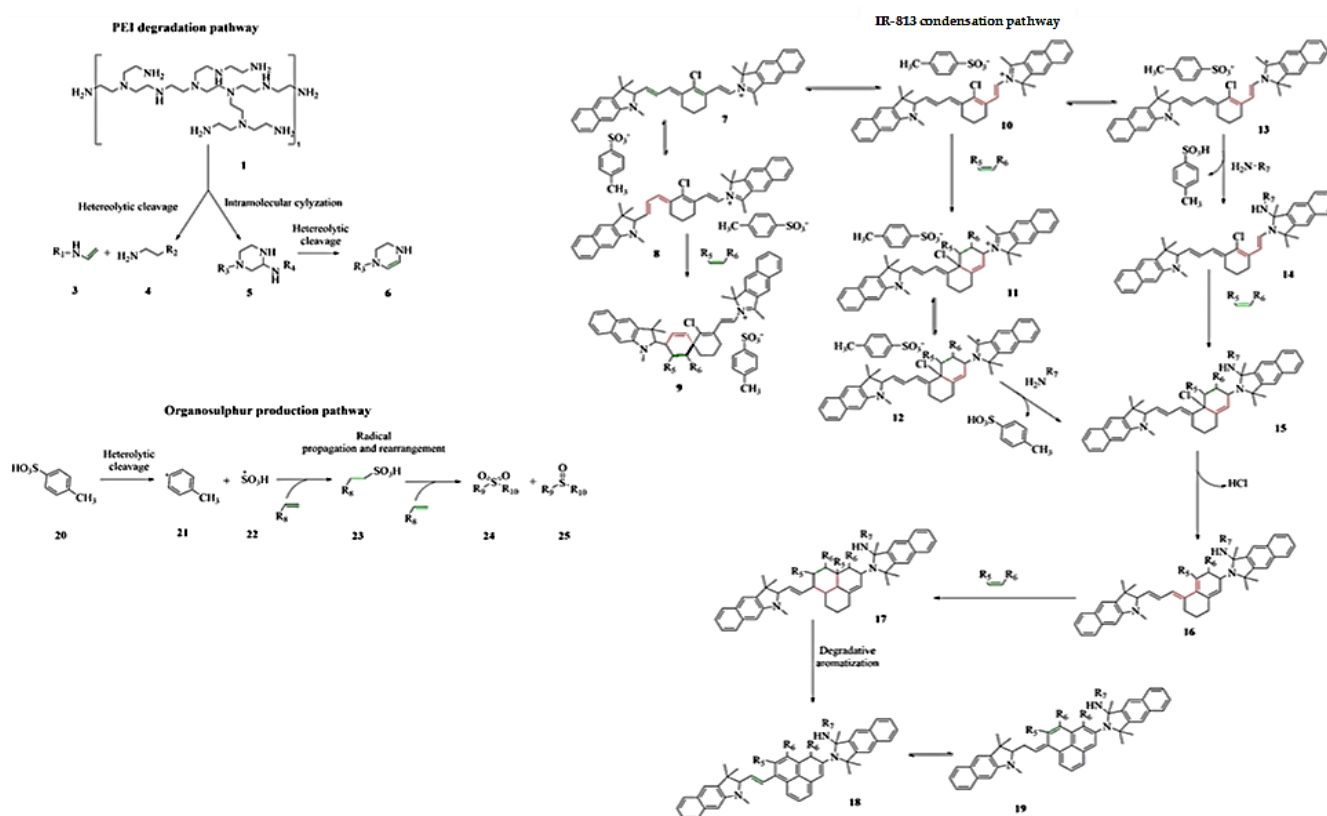

Figure 7. Formation mechanism of 813-CDs.

The PEI degradation is well described in the literature, as reported by Kosheleva et al. [74]. with two possible degradative mechanisms under thermal stimuli. The heterolytic cleavage of PEI promotes the formation of terminal alkenes (**2**) and primary amines (**3**) while the intramolecular cyclization promotes the production of piperazine derivatives (**5–6**). The IR-813 evolution is more complex, and it is based on cycloaddition, nucleophilic additions, and the aromatization process. Firstly, we observed that the pathway that converts **7** into **9** through cycloaddition is not favorable due to the spiro [5.5] undecane moieties (**9**) that are a great stress point for the whole structure.

The equilibrium from 7 to **10** forms cis-diene that could condense producing **12** or reaching the equilibrium with **13**. Both **12** and **13** contain a tertiary carbocation that could be a center for nucleophilic addition of amine groups producing the key intermediate **15**. This species could be rearranged through aromatization forming **18** and **19** that are representative of the ramification of the 813-CDs structure, where the link center based on IR-813 is combined with PEI fragments and other IR-813-based units. Furthermore, protonated tosyl species (**20**) could undergo a heterolytic radical cleavage forming **21** and **22**. Sulfanyl species could promote radical condensation leading to the formation of organic highly oxidized organosulphur compounds (**24** and **25**) properly inserted in the 813-CDs.

The zeta potential of the 813-CD-600 PEI was obtained to further understand both the surface moiety and the surface charge (Table 2). This technique is vital when elucidating the colloidal stability of CDs in various solvents. To preface, an absolute value above 20 mV typically results in CDs that participate in interparticle repulsion [75], effectively producing a well-dispersed colloidal solution. The 813-CD-600 PEI was found to have a negative potential of -5.11 mV, which suggests that the CDs are composed of negative functional groups such as carboxylic and sulfates on the surface attributed to the functionality left by IR-813 (Figure S6A). Hence, the zeta potential data suggests that the CDs will experience the formation of aggregates in solution, meaning an observation of the aggregates by both the TEM and AFM measurements. A zeta potential analysis of 813-CD 25K PEI revealed a value of +18.8 mV, which corresponds to prior data that postulated that this CD had an increased amount of surface amines that contributed to the positive charge of the material (Figure S6B). Furthermore, the value of the zeta potential suggested that there would be uniformity among the CDs with very little aggregation, as confirmed by both TEM and AFM measurements.

Table 2. Zeta potential of respective 813-CDs.

Carbon Dots	Zeta Potential (mV)
813-CD-600 PEI	-5.11 mV
813-CD-25K PEI	+18.8 mV

The TEM images were studied regarding 813-CDs to understand the X$-$Y plane size distribution. The sample was sonicated for 15 min prior to measurement to break down any aggregate formation. Analysis indicated that the 813-CD 600 PEI showed a narrow size distribution of 3.0–10.0 nm with a mean size of 5.5 nm (Figure 8A). Additionally, the histogram determined a particle count of over 50 particles with an acceptable degree of uniformity (Figure 8B). The AFM was also performed on the 813-CDs to understand the height profile of the CDs in the z-axis (Figure 8C). The AFM images show that the 813-CD 600 PEI particles are 6$-$6.5 nm in height, consistent with the previous TEM diameter distribution and confirming the quasi-spherical structure of the 813-CDs. To our surprise, the TEM measurements 813-CD 25K PEI revealed a much smaller and more uniformed narrow size distribution of 2–3.5 nm with a mean size of 2.8 nm (Figure 8D). The histogram of over 500 particles indicates a large degree of uniformity (Figure 8E). These results agree with the AFM measurements which indicate a height profile of roughly 1–2.6 nm (Figure 8F). We propose that the stark difference in size of 813-CD 25K PEI is due to the nature of the larger chained polymer. Specifically, the polymer encases the IR-813 dye during the synthetic process and acts as a barrier to discourage the high degree of carbonization resulting in a smaller particle size, as reported in the literature [76]. In contrast, 813-CD 600 PEI, having a smaller chained polymer, offers less protection; therefore, resulting in a higher degree of carbonization that increases the particle size of the respective CDs.

3.4. Synthesis of 813-CD/PVP Nanocomposite Film

The detailed preparation of 813-CD/PVP nanocomposite thin films were described in Section 2. To assess the solid-state fluorescence of the CDs locked in the PVP polymer matrix, a 535 nm laser was used as a source of excitation onto the 813-CD/PVP film. When light was placed incident onto the face of the thin film, a qualitative bright-orange fluorescence was observed immediately. This phenomenon can be attributed to the absorbance of light by 813-CDs which then emit photons at a longer wavelength, as proposed in Figure 9A. This is in agreement with the literature, which confirms that typical organic fluorophores locked in polymer matrices can attain high optical efficiency due to the spacing of the molecules, discouraging FRET or self-quenching [77–79]. The SEM is a vital tool to elucidate the morphology of the material. As seen in the SEM image (Figure 9B), structural modifications take place in the sample due to interactions of 813-CDs with PVP to produce a surface with

minimal defects. The PL of the film produced peaks at both 600 and 650 nm, respectively under 540 nm excitation (Figure 9C).
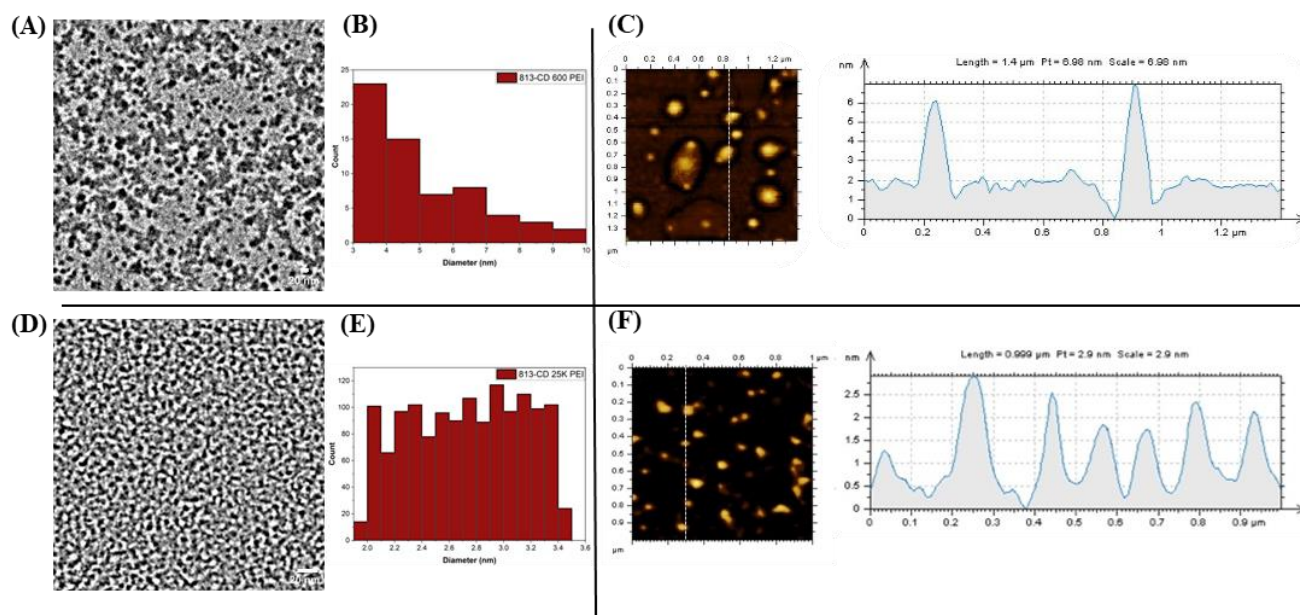

Figure 8. TEM and AFM measurements of 813-CDs. (**A**) TEM of 813-CD-600 PEI. (**B**) AFM scan of 813-CD-600 PEI. (**C**) Histogram of 813-CD-600 PEI. (**D**) TEM of 813-CD-25K PEI. (**E**) AFM measurement of 813-CD-25K PEI. (**F**) Histogram of 813-CD-25K PEI.
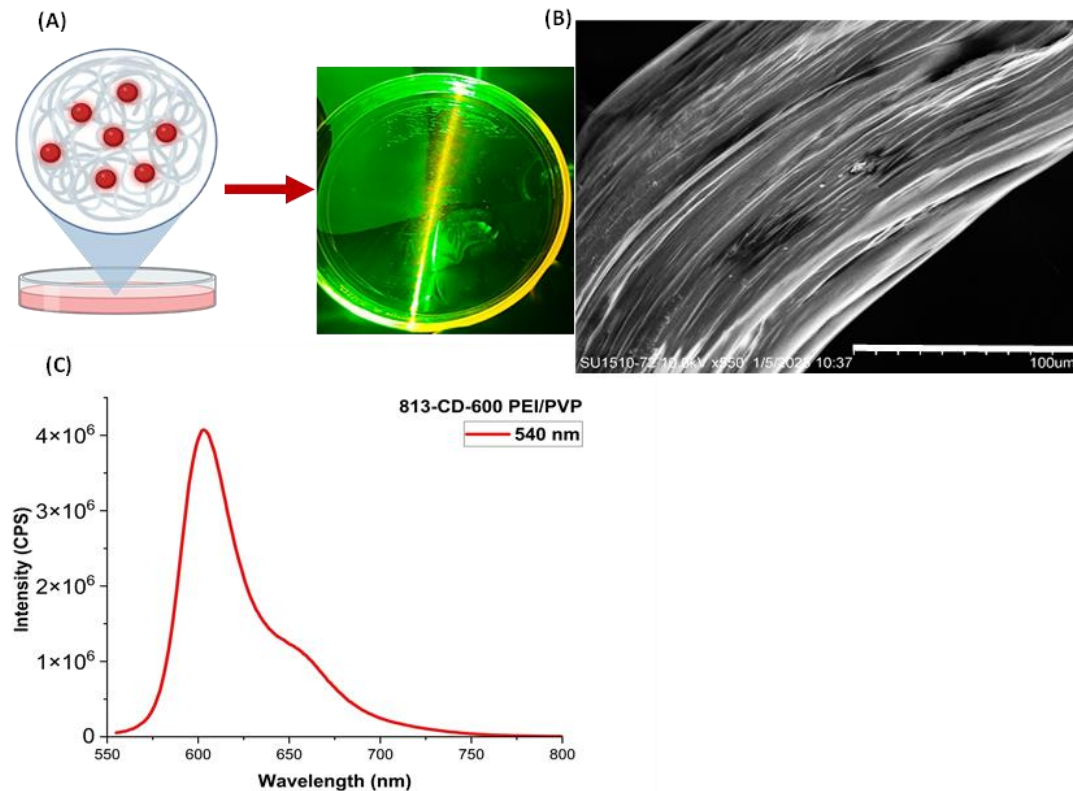

Figure 9. (**A**) Graphical representation and qualitative assessment of 813-CD/PVP nanocomposite thin films on a glass petri dish under 535 nm excitation. Created with BioRender.com, accessed on 1 January 2023. (**B**) SEM measurement of 813-CD/PVP nanocomposite thin film. (**C**) PL spectrum of 813-CD/PVP nanocomposite thin film under 540 nm excitation.

3.5. Cyclic Voltammetry Assessment of 813-CD

The electrochemical behavior of 813-CD as a doping agent for PVP nanocomposites were assessed for applications towards the potential of being used as a coating additive for cathodes to enhance electrochemical performance. In this respect, the literature has shown that PVP film coatings are utilized as additives for a reducing agent to obtain improved stability and rate of lithium ion batteries [80,81]. The presence of these peaks corroborates the n-type nature of our 813-CDs motifs, and are likely a product of the direct reduction of discrete components within the CDs, such as -NH_2 from PEI which coats the surfaces [82–85]. The analyzed system displayed two distinct cathodic peaks at −0.11 V (E_{pi1}) and −0.51 V (E_{pi2}). These electrochemical signals indicate that the 813-CDs feature two distinct electronic states under electronically reducing conditions (Figure 10A). The respective oxidation peaks were observed at 0.43 V(E_{pi3}) and −0.45 V (E_{pi4}) in the reverse scan sweep. Additionally, the stability of 813-CDs was assessed in cycle scans to understand its usability as an additive for PVP coatings for cathodes. To our surprise, the steady decrease of redox peak intensities was not noticeably significant over time (Figure 10B). We suggest that due to the increased stability of our 813-CDs and the strong secondary interactions that exist in the system, no major structural reconfiguration occurs as a function of potential applied, a feature indicative of electrochemical stability [84–86].
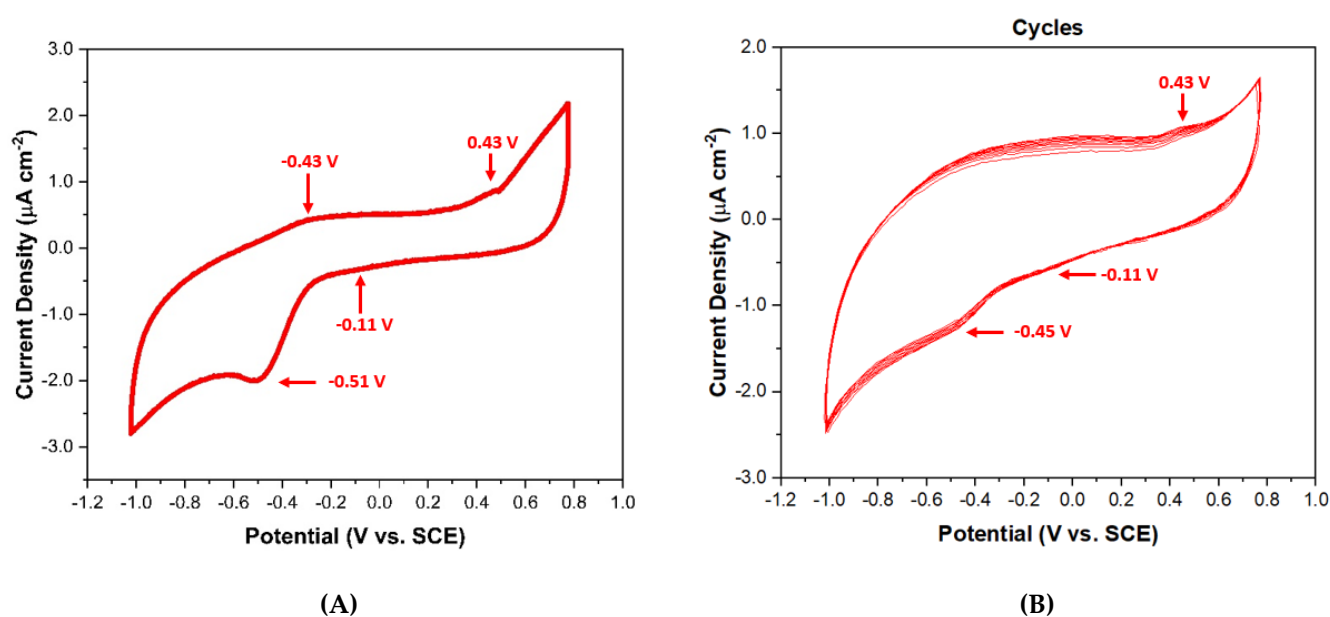

(A)   **(B)**

Figure 10. Cyclic voltammograms of 10 μg/mL of 813-CDs (**A**) at 25 mV/s scan rate (**B**) in repeat cycles recorded in H_2O using 0.1 M NaCl as supporting electrolyte, glassy carbon (GC) electrode as working electrode, Ag/AgCl as reference electrode, and a Pt wire as a counter electrode.

4. Conclusions

For the first time, we have synthesized a new type of red-emitting CDs that have been derived from the organic fluorophore IR-813. Our studies have found that the red emission is attributed to the decrease of conjugation of the fluorophore moieties that passivate the CD alongside emissive states derived from PEI. Further, we prove that the 813-CDs can be applicable in solvent polarity sensing, as well as inducing a bathochromic shift in water. A summary of the synthetic protocols and properties for each CD is provided in Table S1. Additionally, this is the first report of far-red emissive CD/PVP nanocomposite films with solid state emission. To our surprise, the CV assessment of the 813-CDs concludes that this material is suitable as a doping agent to increase the electrochemical behavior of PVP to be potentially applied as a dopant for cathode film coating. In further application, we believe that the results of our far-red emissive carbon dots are highly favorable. The prospects of 813-CDs in vivo are of utmost importance moving forward to assess the cytotoxicity in cell

lines. We are hopeful that once validated, our CDs are to be used as theranostic agents to both image and deliver drugs in vivo with live fluorescence tracking. Recent work from our group involving cationic CDs has shown the capabilities of positively charged CDs to bind with DNA both through electrostatic and intercalative modes [87]. We hypothesize in this regard that our CDs may be applicable in this field of study in future works.

Supplementary Materials: The following supporting information can be downloaded at: https://www.mdpi.com/article/10.3390/molecules28041755/s1, Figure S1: Graphic illustration of 813-CD synthetic procedure; Figure S2: Images of 813-CDs post-synthesis and purification. (A) Image of 813-CD 600 PEI. (B) Image of 813-CD 25K PEI; Figure S3: PL spectra of 813-CD versus IR-813. (A) PL spectrum of IR-813 from 400–800 nm in methanol. (B) PL spectrum of IR-813 from 750–900 nm in methanol. (C) PL spectrum of 813-CD from 400–800 nm in water; Figure S4: Optical analysis of 813-CDs in various solvents of decreasing polarities according to the solvent polarity index (P), PL spectrum. (A) water P:1.00, (B) ethanol P:0.654, (C) acetic acid P:0.648, (D) DMSO P:0.444, (E) DMF P:0.386, (F) methylene chloride P:0.309, (G) chloroform P:0.259, (H) ethyl acetate P:0.228, (I) ether P:0.117, (J) toluene P:0.099, and (K) hexane P:0.009, respectively. (L) 813-CDs in water under excitation at 535 nm; Figure S5: UV-vis absorbance spectra of 813-CDs in water. (A) UV-vis spectrum of 813-CD 25K PEI from 200–800 nm. (B) UV-vis spectrum of 813-CD 600 PEI from 200–800 nm; Figure S6: Zeta potential of 813-CDs. (A) Zeta potential of 813-CD 600 PEI, -5.11 mV. (B) Zeta potential of 813-CD 25K PEI, $+18.8$ mV.; Table S1: Summary of CD methodology and properties.

Author Contributions: Conceptualization, J.B.D. and R.M.L.; methodology, J.B.D., B.C.L.B.F., Y.Z., W.Z., V.P., J.C., J.B.D. and E.C.; validation, J.B.D. and R.M.L.; formal analysis, J.B.D., B.C.L.B.F., Y.Z., W.Z., Q.J., J.C. and E.C.; investigation, J.B.D., E.C. and R.M.L.; resources, M.B., B.P.S.C., J.-H.O. and A.T.; data curation, J.B.D. and E.C.; writing—original draft preparation, J.B.D.; writing—review and editing, J.B.D., R.M.L.,B.C.L.B.F., Y.Z., W.Z., V.P., J.C. and E.C.; visualization, J.B.D. and R.M.L.; supervision, R.M.L.; project administration, R.M.L.; funding acquisition, R.M.L. All authors have read and agreed to the published version of the manuscript.

Institutional Review Board Statement: Not applicable.

Informed Consent Statement: Not applicable.

Data Availability Statement: Not applicable.

Conflicts of Interest: The authors declare no conflict of interest.

References

1. Bai, Y.; Zhao, J.; Wang, S.; Lin, T.; Ye, F.; Zhao, S. Carbon Dots with Absorption Red-Shifting for Two-Photon Fluorescence Imaging of Tumor Tissue pH and Synergistic Phototherapy. *ACS Appl. Mater. Interfaces* **2021**, *13*, 35365–35375. [CrossRef]
2. Wen, Y.; Jia, Q.; Nan, F.; Zheng, X.; Liu, W.; Wu, J.; Ren, H.; Ge, J.; Wang, P. Pheophytin Derived Near-Infrared-Light Responsive Carbon Dot Assembly as a New Phototheranotic Agent for Bioimaging and Photodynamic Therapy. *Chem. Asian J.* **2019**, *14*, 2162–2168. [CrossRef] [PubMed]
3. Sun, S.; Chen, J.; Jiang, K.; Tang, Z.; Wang, Y.; Li, Z.; Liu, C.; Wu, A.; Lin, H. Ce6-Modified Carbon Dots for Multimodal-Imaging-Guided and Single-NIR-Laser-Triggered Photothermal/Photodynamic Synergistic Cancer Therapy by Reduced Irradiation Power. *ACS Appl. Mater. Interfaces* **2019**, *11*, 5791–5803. [CrossRef]
4. Du, J.; Xu, N.; Fan, J.; Sun, W.; Peng, X. Carbon Dots for In Vivo Bioimaging and Theranostics. *Small* **2019**, *15*, e1805087. [CrossRef] [PubMed]
5. Wang, J.; Zhang, P.; Huang, C.; Liu, G.; Leung, K.C.-F.; Wáng, Y.X.J. High Performance Photoluminescent Carbon Dots for In Vitro and In Vivo Bioimaging: Effect of Nitrogen Doping Ratios. *Langmuir* **2015**, *31*, 8063–8073. [CrossRef]
6. Yang, S.-T.; Cao, L.; Luo, P.G.; Lu, F.; Wang, X.; Wang, H.; Meziani, M.J.; Liu, Y.; Qi, G.; Sun, Y.-P. Carbon Dots for Optical Imaging In Vivo. *J. Am. Chem. Soc.* **2009**, *131*, 11308–11309. [CrossRef] [PubMed]
7. He, C.; Lin, X.; Mei, Y.; Luo, Y.; Yang, M.; Kuang, Y.; Yi, X.; Zeng, W.; Huang, Q.; Zhong, B. Recent Advances in Carbon Dots for In Vitro/Vivo Fluorescent Bioimaging: A Mini-Review. *Front. Chem.* **2022**, *10*, 905475. [CrossRef]
8. Ji, C.; Zhou, Y.; Leblanc, R.M.; Peng, Z. Recent Developments of Carbon Dots in Biosensing: A Review. *ACS Sensors* **2020**, *5*, 2724–2741. [CrossRef] [PubMed]

9. Zhou, Y.; Mintz, K.J.; Sharma, S.K.; Leblanc, R.M. Carbon Dots: Diverse Preparation, Application, and Perspective in Surface Chemistry. *Langmuir* **2019**, *35*, 9115–9132. [CrossRef] [PubMed]

10. Wu, J.; Chen, G.; Jia, Y.; Ji, C.; Wang, Y.; Zhou, Y.; Leblanc, R.M.; Peng, Z. Carbon dot composites for bioapplications: A review. *J. Mater. Chem. B* **2022**, *10*, 843–869. [CrossRef] [PubMed]

11. Peng, Z.; Miyanji, E.H.; Zhou, Y.; Pardo, J.; Hettiarachchi, S.D.; Li, S.; Blackwelder, P.L.; Skromne, I.; Leblanc, R.M. Carbon dots: Promising biomaterials for bone-specific imaging and drug delivery. *Nanoscale* **2017**, *9*, 17533–17543. [CrossRef]

12. Gavalas, S.; Kelarakis, A. Towards Red Emissive Systems Based on Carbon Dots. *Nanomaterials* **2021**, *11*, 2089. [CrossRef]

13. Zhao, M.; Guo, Y.-S.; Xu, W.-N.; Zhao, Y.-F.; Xie, H.-Y.; Li, H.-J.; Chen, X.-F.; Zhao, R.-S.; Guo, D.-S. Far-red to near-infrared fluorescent probes based on silicon-substituted xanthene dyes for sensing and imaging. *TrAC Trends Anal. Chem.* **2020**, *122*, 115704. [CrossRef]

14. Jun, Y.W.; Kim, H.R.; Reo, Y.J.; Dai, M.; Ahn, K.H. Addressing the autofluorescence issue in deep tissue imaging by two-photon microscopy: The significance of far-red emitting dyes. *Chem. Sci.* **2017**, *8*, 7696–7704. [CrossRef] [PubMed]

15. Wang, J.; Zhu, Y.; Wang, L. Synthesis and Applications of Red-Emissive Carbon Dots. *Chem. Rec.* **2019**, *19*, 2083–2094. [CrossRef] [PubMed]

16. Ge, J.; Jia, Q.; Liu, W.; Guo, L.; Liu, Q.; Lan, M.; Zhang, H.; Meng, X.; Wang, P. Red-Emissive Carbon Dots for Fluorescent, Photoacoustic, and Thermal Theranostics in Living Mice. *Adv. Mater.* **2015**, *27*, 4169–4177. [CrossRef] [PubMed]

17. Sun, S.; Zhang, L.; Jiang, K.; Wu, A.; Lin, H. Toward High-Efficient Red Emissive Carbon Dots: Facile Preparation, Unique Properties, and Applications as Multifunctional Theranostic Agents. *Chem. Mater.* **2016**, *28*, 8659–8668. [CrossRef]

18. Gao, D.; Zhao, H.; Chen, X.; Fan, H. Recent advance in red-emissive carbon dots and their photoluminescent mechanisms. *Mater. Today Chem.* **2018**, *9*, 103–113. [CrossRef]

19. Hallaji, Z.; Bagheri, Z.; Kalji, S.-O.; Ermis, E.; Ranjbar, B. Recent advances in the rational synthesis of red-emissive carbon dots for nanomedicine applications: A review. *Flatchem* **2021**, *29*, 100271. [CrossRef]

20. Yang, X.; Ai, L.; Yu, J.; Waterhouse, G.I.N.; Sui, L.; Ding, J.; Zhang, B.; Yong, X.; Lu, S. Photoluminescence mechanisms of red-emissive carbon dots derived from non-conjugated molecules. *Sci. Bull.* **2022**, *67*, 1450–1457. [CrossRef]

21. Apter, B.; Lapshina, N.; Barhom, H.; Fainberg, B.; Handelman, A.; Accardo, A.; Diaferia, C.; Ginzburg, P.; Morelli, G.; Rosenman, G. Fluorescence Phenomena in Amyloid and Amyloidogenic Bionanostructures. *Crystals* **2020**, *10*, 668. [CrossRef]

22. Tauc, J. Optical properties and electronic structure of amorphous Ge and Si. *Mater. Res. Bull.* **1968**, *3*, 37–46. [CrossRef]

23. Ren, J.; Malfatti, L.; Enzo, S.; Carbonaro, C.M.; Calvillo, L.; Granozzi, G.; Innocenzi, P. Boron oxynitride two-colour fluorescent dots and their incorporation in a hybrid organic-inorganic film. *J. Colloid Interface Sci.* **2020**, *560*, 398–406. [CrossRef]

24. Kundelev, E.V.; Tepliakov, N.V.; Leonov, M.Y.; Maslov, V.G.; Baranov, A.V.; Fedorov, A.V.; Rukhlenko, I.D.; Rogach, A.L. Towards Bright Red-Emissive Carbon Dots through Controlling Interaction among Surface Emission Centers. *J. Phys. Chem. Lett.* **2020**, *11*, 8121–8127. [CrossRef]

25. Reckmeier, C.J.; Wang, Y.; Zboril, R.; Rogach, A.L. Influence of Doping and Temperature on Solvatochromic Shifts in Optical Spectra of Carbon Dots. *J. Phys. Chem. C* **2016**, *120*, 10591–10604. [CrossRef]

26. Alaş, M.; Genç, R. Solvatochromic Surface-Passivated Carbon Dots for Fluorometric Moisture Sensing in Organic Solvents. *ACS Appl. Nano Mater.* **2021**, *4*, 7974–7987. [CrossRef]

27. Basu, N.; Mandal, D. Solvatochromic Response of Carbon Dots: Evidence of Solvent Interaction with Different Types of Emission Centers. *J. Phys. Chem. C* **2018**, *122*, 18732–18741. [CrossRef]

28. Wang, H.; Haydel, P.; Sui, N.; Wang, L.; Liang, Y.; Yu, W.W. Wide emission shifts and high quantum yields of solvatochromic carbon dots with rich pyrrolic nitrogen. *Nano Res.* **2020**, *13*, 2492–2499. [CrossRef]

29. Vijeata, A.; Chaudhary, G.R.; Umar, A.; Chaudhary, S. Distinctive Solvatochromic Response of Fluorescent Carbon Dots Derived from Different Components of Aegle Marmelos Plant. *Eng. Sci.* **2021**, *15*, 197–209. [CrossRef]

30. Kundu, A.; Park, B.; Oh, J.; Sankar, K.V.; Ray, C.; Kim, W.S.; Jun, S.C. Multicolor emissive carbon dot with solvatochromic behavior across the entire visible spectrum. *Carbon* **2020**, *156*, 110–118. [CrossRef]

31. Zhu, X.; Wang, J.; Zhu, Y.; Jiang, H.; Tan, D.; Xu, Z.; Mei, T.; Li, J.; Xue, L.; Wang, X. Green emitting N,S-co-doped carbon dots for sensitive fluorometric determination of Fe(III) and Ag(I) ions, and as a solvatochromic probe. *Microchim. Acta* **2018**, *185*, 510. [CrossRef] [PubMed]

32. Arshad, F.; Pal, A.; Rahman, M.A.; Ali, M.; Khan, J.A.; Sk, M.P. Insights on the solvatochromic effects in N-doped yellow-orange emissive carbon dots. *New J. Chem.* **2018**, *42*, 19837–19843. [CrossRef]

33. Ishchenko, A.A.; Kulinich, A.V.; Bondarev, S.L.; Knyukshto, V.N. Electronic structure and fluorescent properties of malononitrile-based merocyanines with positive and negative solvatochromism. *Opt. Spectrosc.* **2008**, *104*, 57–68. [CrossRef]

34. Domínguez, M.; Rezende, M.C. Towards a unified view of the solvatochromism of phenolate betaine dyes. *J. Phys. Org. Chem.* **2010**, *23*, 156–170. [CrossRef]

35. Ren, J.; Sun, J.; Sun, X.; Song, R.; Xie, Z.; Zhou, S. Precisely Controlled Up/Down-Conversion Liquid and Solid State Photoluminescence of Carbon Dots. *Adv. Opt. Mater.* **2018**, *6*, 1800115. [CrossRef]

36. Yoshinaga, T.; Shinoda, M.; Iso, Y.; Isobe, T.; Ogura, A.; Takao, K.-I. Glycothermally Synthesized Carbon Dots with Narrow-Bandwidth and Color-Tunable Solvatochromic Fluorescence for Wide-Color-Gamut Displays. *ACS Omega* **2021**, *6*, 1741–1750. [CrossRef] [PubMed]

37. Badawi, A. Enhancement of the optical properties of PVP using Zn1-xSnxS for UV-region optical applications. *Appl. Phys. A* **2021**, *127*, 1–9. [CrossRef]

38. Agool, I.R.; Kadhim, K.J.; Hashim, A. Synthesis of (PVA–PEG–PVP–ZrO2) nanocomposites for energy release and gamma shielding applications. *Int. J. Plast. Technol.* **2017**, *21*, 444–453. [CrossRef]

39. Carotenuto, G.; Pepe, G.P.; Nicolais, L. Preparation and characterization of nano-sized Ag/PVP composites for optical applications. *Eur. Phys. J. B* **2000**, *16*, 11–17. [CrossRef]

40. Husain, M.S.B.; Gupta, A.; Alashwal, B.Y.; Sharma, S. Synthesis of PVA/PVP based hydrogel for biomedical applications: A review. *Energy Sources Part A Recover. Util. Environ. Eff.* **2018**, *40*, 2388–2393. [CrossRef]

41. Rao, C.V.S.; Ravi, M.; Raja, V.; Bhargav, P.B.; Sharma, A.K.; Rao, V.V.R.N. Preparation and characterization of PVP-based polymer electrolytes for solid-state battery applications. *Iran. Polym. J.* **2012**, *21*, 531–536. [CrossRef]

42. Teodorescu, M.; Bercea, M.; Morariu, S. Biomaterials of PVA and PVP in medical and pharmaceutical applications: Perspectives and challenges. *Biotechnol. Adv.* **2019**, *37*, 109–131. [CrossRef] [PubMed]

43. Lochhead, R.Y. The Role of Polymers in Cosmetics: Recent Trends. In *Cosmetic Nanotechnology*; ACS Symposium Series; American Chemical Society: Hattiesburg, MS, USA, 2007; Volume 961, pp. 3–56.

44. Feng, T.; Zhu, S.; Zeng, Q.; Lu, S.; Tao, S.; Liu, J.; Yang, B. Supramolecular Cross-Link-Regulated Emission and Related Applications in Polymer Carbon Dots. *ACS Appl. Mater. Interfaces* **2018**, *10*, 12262–12277. [CrossRef]

45. Yan, F.; Zhang, H.; Xu, J.; Wu, Y.; Zang, Y.; Sun, J. Color Emission Carbon Dots with Quench-ResixAstant Solid-State Fluorescence for Light-Emitting Diodes. *ACS Sustain. Chem. Eng.* **2021**, *9*, 3901–3908. [CrossRef]

46. Ren, J.; Stagi, L.; Innocenzi, P. Fluorescent carbon dots in solid-state: From nanostructures to functional devices. *Prog. Solid State Chem.* **2021**, *62*, 100295. [CrossRef]

47. Javanbakht, S.; Namazi, H. Solid state photoluminescence thermoplastic starch film containing graphene quantum dots. *Carbohydr. Polym.* **2017**, *176*, 220–226. [CrossRef] [PubMed]

48. Arshad, F.; Pal, A.; Sk, M.P. Review—Aggregation-Induced Emission in Carbon Dots for Potential Applications. *ECS J. Solid State Sci. Technol.* **2021**, *10*, 021001. [CrossRef]

49. Li, H.; Su, D.; Gao, H.; Yan, X.; Kong, D.; Jin, R.; Liu, X.; Wang, C.; Lu, G. Design of Red Emissive Carbon Dots: Robust Performance for Analytical Applications in Pesticide Monitoring. *Anal. Chem.* **2020**, *92*, 3198–3205. [CrossRef] [PubMed]

50. Havrdova, M.; Hola, K.; Skopalik, J.; Tománková, K.; Petr, M.; Cepe, K.; Polakova, K.; Tucek, J.; Bourlinos, A.B.; Zboril, R. Toxicity of carbon dots-Effect of surface functionalization on the cell viability, reactive oxygen species generation and cell cycle. *Carbon* **2016**, *99*, 238–248. [CrossRef]

51. Moghimi, S.M.; Symonds, P.; Murray, J.C.; Hunter, A.C.; Debska, G.; Szewczyk, A.C. A two-stage poly(ethylenimine)-mediated cytotoxicity: Implications for gene transfer/therapy. *Mol. Ther.* **2005**, *11*, 990–995. [CrossRef]

52. Iida, T.; Mori, T.; Katayama, Y.; Niidome, T. Overall interaction of cytosolic proteins with the PEI/DNA complex. *J. Control. Release* **2007**, *118*, 364–369. [CrossRef]

53. Kircheis, R.; Wightman, L.; Wagner, E. Design and gene delivery activity of modified polyethylenimines. *Adv. Drug Deliv. Rev.* **2001**, *53*, 341–358. [CrossRef]

54. Wang, C.; Xu, Z.; Zhang, C. Polyethyleneimine-Functionalized Fluorescent Carbon Dots: Water Stability, pH Sensing, and Cellular Imaging. *Chemnanomat* **2015**, *1*, 122–127. [CrossRef]

55. Yin, J.-Y.; Liu, H.-J.; Jiang, S.; Chen, Y.; Yao, Y. Hyperbranched Polymer Functionalized Carbon Dots with Multistimuli-Responsive Property. *ACS Macro Lett.* **2013**, *2*, 1033–1037. [CrossRef] [PubMed]

56. Ashcraft, A.; Liu, K.; Mukhopadhyay, A.; Paulino, V.; Liu, C.; Bernard, B.; Husainy, D.; Phan, T.; Olivier, J.-H.H. A Molecular Strategy to Lock-in the Conformation of a Perylene Bisimide-Derived Supramolecular Polymer. *Angew. Chem. Int. Ed.* **2020**, *59*, 7487–7493. [CrossRef] [PubMed]

57. Zhou, Y.; Zahran, E.M.; Quiroga, B.A.; Perez, J.; Mintz, K.J.; Peng, Z.; Liyanage, P.Y.; Pandey, R.R.; Chusuei, C.C.; Leblanc, R.M. Size-dependent photocatalytic activity of carbon dots with surface-state determined photoluminescence. *Appl. Catal. B Environ.* **2019**, *248*, 157–166. [CrossRef] [PubMed]

58. Hettiarachchi, S.D.; Graham, R.M.; Mintz, K.J.; Zhou, Y.; Vanni, S.; Peng, Z.; Leblanc, R.M. Triple conjugated carbon dots as a nano-drug delivery model for glioblastoma brain tumors. *Nanoscale* **2019**, *11*, 6192–6205. [CrossRef] [PubMed]

59. Liu, E.; Li, D.; Zhou, X.; Zhou, G.; Xiao, H.; Zhou, D.; Tian, P.; Guo, R.; Qu, S. Highly Emissive Carbon Dots in Solid State and Their Applications in Light-Emitting Devices and Visible Light Communication. *ACS Sustain. Chem. Eng.* **2019**, *7*, 9301–9308. [CrossRef]

60. Xu, X.; Cai, L.; Hu, G.; Mo, L.; Zheng, Y.; Hu, C.; Lei, B.; Zhang, X.; Liu, Y.; Zhuang, J. Red-emissive carbon dots from spinach: Characterization and application in visual detection of time. *J. Lumin.* **2020**, *227*, 117534. [CrossRef]

61. Hu, Y.; Al Awak, M.M.; Yang, F.; Yan, S.; Xiong, Q.; Wang, P.; Tang, Y.; Yang, L.; LeCroy, G.E.; Hou, X.; et al. Photoexcited state properties of carbon dots from thermally induced functionalization of carbon nanoparticles. *J. Mater. Chem. C* **2016**, *4*, 10554–10561. [CrossRef] [PubMed]

62. Li, R.; Wei, F.; Wu, X.; Zhou, P.; Chen, Q.; Cen, Y.; Xu, G.; Cheng, X.; Zhang, A.; Hu, Q. PEI modified orange emissive carbon dots with excitation-independent fluorescence emission for cellular imaging and siRNA delivery. *Carbon* **2021**, *177*, 403–411. [CrossRef]

63. Ru, Y.; Waterhouse, G.I.N.; Lu, S. Aggregation in carbon dots. *Aggregate* **2022**, *3*, e296. [CrossRef]

64. Nigam, S.; Rutan, S. Principles and Applications of Solvatochromism. *Appl. Spectrosc.* **2001**, *55*, 362A–370A. [CrossRef]

65. de Melo, C.E.A.; Nandi, L.G.; Domínguez, M.; Rezende, M.C.; Machado, V.G. Solvatochromic behavior of dyes with dimethyl-lamino electron-donor and nitro electron-acceptor groups in their molecular structure. *J. Phys. Org. Chem.* **2015**, *28*, 250–260. [CrossRef]

66. Reichardt, C. Solvatochromic Dyes as Solvent Polarity Indicators. *Chem. Rev.* **1994**, *94*, 2319–2358. [CrossRef]

67. Yang, Z.; Li, H.; Xu, T.; She, M.; Chen, J.; Jia, X.; Liu, P.; Liu, X.; Li, J. Red emissive carbon dots as a fluorescent sensor for fast specific monitoring and imaging of polarity in living cells. *J. Mater. Chem. A* **2023**, *11*, 2679–2689. [CrossRef]

68. Liu, J.; Li, R.; Yang, B. Carbon Dots: A New Type of Carbon-Based Nanomaterial with Wide Applications. *ACS Cent. Sci.* **2020**, *6*, 2179–2195. [CrossRef] [PubMed]

69. Zhu, S.; Song, Y.; Zhao, X.; Shao, J.; Zhang, J.; Yang, B. The photoluminescence mechanism in carbon dots (graphene quantum dots, carbon nanodots, and polymer dots): Current state and future perspective. *Nano Res.* **2015**, *8*, 355–381. [CrossRef]

70. Yan, F.; Sun, Z.; Zhang, H.; Sun, X.; Jiang, Y.; Bai, Z. The fluorescence mechanism of carbon dots, and methods for tuning their emission color: A review. *Microchim. Acta* **2019**, *186*, 583. [CrossRef] [PubMed]

71. Kosheleva, I.M.; Gembitskii, P.A.; Chmarin, A.I.; Kolesova, L.M.; Zhuk, D.S.; Kargin, V.A. Some properties and the structure of high-molecular polyethylenimine. *Russ. Chem. Bull.* **1971**, *20*, 1536–1541. [CrossRef]

72. Zhang, Y.; Yang, M.; Portney, N.G.; Cui, D.; Budak, G.; Ozbay, E.; Ozkan, M.; Ozkan, C.S. Zeta potential: A surface electrical characteristic to probe the interaction of nanoparticles with normal and cancer human breast epithelial cells. *Biomed. Microdevices* **2008**, *10*, 321–328. [CrossRef] [PubMed]

73. Xia, C.; Zhu, S.; Feng, T.; Yang, M.; Yang, B. Evolution and Synthesis of Carbon Dots: From Carbon Dots to Carbonized Polymer Dots. *Adv. Sci.* **2019**, *6*, 1901316. [CrossRef] [PubMed]

74. Zhang, Y.; Zhuo, P.; Yin, H.; Fan, Y.; Zhang, J.; Liu, X.; Chen, Z. Solid-State Fluorescent Carbon Dots with Aggregation-Induced Yellow Emission for White Light-Emitting Diodes with High Luminous Efficiencies. *ACS Appl. Mater. Interfaces* **2019**, *11*, 24395–24403. [CrossRef]

75. Wei, S.; Li, Z.; Lu, W.; Liu, H.; Zhang, J.; Chen, T.; Tang, B.Z. Multicolor Fluorescent Polymeric Hydrogels. *Angew. Chem. Int. Ed.* **2021**, *60*, 8608–8624. [CrossRef]

76. Feng, Z.; Adolfsson, K.H.; Xu, Y.; Fang, H.; Hakkarainen, M.; Wu, M. Carbon dot/polymer nanocomposites: From green synthesis to energy, environmental and biomedical applications. *Sustain. Mater. Technol.* **2021**, *29*, e00304. [CrossRef]

77. Gan, Q.; Qin, N.; Zhu, Y.; Huang, Z.; Zhang, F.; Gu, S.; Xie, J.; Zhang, K.; Lu, L.; Lu, Z. Polyvinylpyrrolidone-Induced Uniform Surface-Conductive Polymer Coating Endows Ni-Rich $LiNi_{0.8}Co_{0.1}Mn_{0.1}O_2$ with Enhanced Cyclability for Lithium-Ion Batteries. *ACS Appl. Mater. Interfaces* **2019**, *11*, 12594–12604. [CrossRef]

78. Wang, H.; Lin, J.; Zhang, X.; Wang, L.; Yang, J.; Fan, E.; Wu, F.; Chen, R.; Li, L. Improved Electrochemical Performance of $LiNi_{0.8}Co_{0.1}Mn_{0.1}O_2$ Cathode Materials Induced by a Facile Polymer Coating for Lithium-Ion Batteries. *ACS Appl. Energy Mater.* **2021**, *4*, 6205–6213. [CrossRef]

79. Kaur, G.; Gates, B.D. Review—Surface Coatings for Cathodes in Lithium Ion Batteries: From Crystal Structures to Electrochemical Performance. *J. Electrochem. Soc.* **2022**, *169*, 043504. [CrossRef]

80. Lee, J.-E.; Kim, M.-C.; Moon, S.-H.; Kim, E.-S.; Shin, Y.-K.; Choi, S.; Kwon, S.-H.; Kim, S.-J.; Kwon, H.-J.; Park, K.-W. Role of polyvinylpyrrolidone in the electrochemical performance of Li_2MnO_3 cathode for lithium-ion batteries. *RSC Adv.* **2019**, *9*, 10297–10304. [CrossRef] [PubMed]

81. Li, Y.; Zhao, Y.; Cheng, H.; Hu, Y.; Shi, G.; Dai, L.; Qu, L. Nitrogen-Doped Graphene Quantum Dots with Oxygen-Rich Functional Groups. *J. Am. Chem. Soc.* **2012**, *134*, 15–18. [CrossRef]

82. Hu, S.; Huang, Q.; Lin, Y.; Wei, C.; Zhang, H.; Zhang, W.; Guo, Z.; Bao, X.; Shi, J.; Hao, A. Reduced graphene oxide-carbon dots composite as an enhanced material for electrochemical determination of dopamine. *Electrochim. Acta* **2014**, *130*, 805–809. [CrossRef]

83. Li, Z.; Liu, X.; Wang, L.; Bu, F.; Wei, J.; Pan, D.; Wu, M. Hierarchical 3D All-Carbon Composite Structure Modified with N-Doped Graphene Quantum Dots for High-Performance Flexible Supercapacitors. *Small* **2018**, *14*, 1801498. [CrossRef] [PubMed]

84. Lu, L.; Xie, Y. Phosphomolybdic acid cluster bridging carbon dots and polyaniline nanofibers for effective electrochemical energy storage. *J. Mater. Sci.* **2019**, *54*, 4842–4858. [CrossRef]

85. Wang, L.; Zeng, Q.; Chen, Q.; Li, C.M.; Chen, J. Synergistically boosting the electrochemical performance of polypyrrole-coated activated carbon derived from carbon dots for a high-performance supercapacitor. *Chem. Commun.* **2021**, *57*, 9264–9267. [CrossRef] [PubMed]

86. Xie, F.; Zhou, M.; Wang, G.; Wang, Q.; Yan, M.; Bi, H. Morphology-dependent electrochemical performance of nitrogen-doped carbon dots@polyaniline hybrids for supercapacitors. *Int. J. Energy Res.* **2019**, *43*, 7529–7540. [CrossRef]

87. Chen, J.; Li, F.; Gu, J.; Zhang, X.; Bartoli, M.; Domena, J.B.; Zhou, Y.; Zhang, W.; Paulino, V.; Ferreira, B.C.L.B.; et al. Cancer cells inhibition by cationic carbon dots targeting the cellular nucleus. *J. Colloid Interface Sci.* **2023**, *637*, 193–206. [CrossRef] [PubMed]